PHYSICAL REVIEW B **86**, 020507(R) (2012)

Competing many-body instabilities and unconventional superconductivity in graphene

Maximilian L. Kiesel,[1] Christian Platt,[1] Werner Hanke,[1] Dmitry A. Abanin,[2] and Ronny Thomale[1,3]
[1]*Institute for Theoretical Physics, University of Würzburg, Am Hubland, D-97074 Würzburg, Germany*
[2]*Department of Physics, Harvard University, Cambridge, Massachusetts 02138, USA*
[3]*Department of Physics, Stanford University, Stanford, California 94305, USA*
(Received 31 October 2011; published 30 July 2012)

The band structure of graphene exhibits van Hove singularities (VHSs) at dopings $x = \pm 1/8$ away from the Dirac point. Near the VHS, interactions effects, enhanced due to the large density of states, can give rise to various many-body phases. We study the competition between many-body instabilities in graphene using the functional renormalization group. We predict a rich phase diagram, which, depending on band structure as well as the range and scale of Coulomb interactions, contains a $d + id$-wave superconducting (SC) phase, or a spin-density-wave phase at the VHS. The $d + id$ state is expected to exhibit quantized charge and spin Hall response, as well as Majorana modes bound to vortices. Nearby the VHS, we find singlet $d + id$-wave and triplet f-wave SC phases.

DOI: 10.1103/PhysRevB.86.020507 PACS number(s): 73.22.Pr, 74.20.Mn, 74.70.Wz

Introduction. Graphene, a monolayer of carbon, hosts a two-dimensional electronic system (2DES) with unique properties.[1] In particular, the Coulomb interaction plays an important role,[2] giving rise to many-body phenomena including marginal Fermi-liquid behavior,[3] energy-dependent renormalization of the Fermi velocity,[4] and many-body quantum Hall states.[1]

Experimentally, graphene offers a high degree of tunability. In particular, carrier density can be controlled in a broad range. Near the Dirac point (filling level of electrons $n = 1/2$), such a control is achieved by back gates and local top gates.[1] Recently, it was demonstrated that chemical doping[5] and electrolytic gating[6] enable doping graphene far away from the Dirac point. In particular, the density can be tuned to the vicinity of the van Hove singularities (VHSs) in the band structure, which occur at fillings $n = 3/8,5/8$. In the case of chemical doping, the dopants form a superlattice on top of the graphene sheet. This strongly reduces the amount of disorder induced by doping. Furthermore, the spacing of the superlattice is so large that hybridization in the dopant layer can be neglected and, hence, transport measurements of the graphene sample remain unaffected.

Before the strong doping of graphene, which has been recently accomplished experimentally, superconductivity had been predominantly studied around the Dirac point. This includes $p + ip$-wave predictions from electron-phonon or plasmonic interactions,[7] Kekule order,[8] and f- or $d + id$-waves from electron-electron[9] interactions. Mean-field theories[10,11] have arrived at $T_c > 1000$ K, with only slightly lower results for variational approaches.[12] Despite these predictions, superconductivity has not been observed in this regime, due to small electronic density of states (DOS) and weak phonon effects.[13]

Near a VHS, opposed to the Dirac point regime, electronic interaction effects are expected to be strongly enhanced due to the logarithmically diverging DOS and near-nested Fermi surface.[5] In this regime, many-body states with appreciable critical temperatures may arise. Possible candidate states include charge-density wave (CDW), a spin-density wave (SDW), or a superconducting (SC) state. The latter has been recently considered within a perturbative three-patch renormalization group (3RG)[14] that only takes into account the saddle points of the Fermi surface. Generally, however, a subtle interplay of kinetic and interaction parameters is expected to decide which many-body instability is preferred at the VHS, which is the subject of this Rapid Communication. For graphene, the additional complication arises that as the bandwidth ($\sim$17 eV) is of the order of the interaction scale ($\sim$10 eV), graphene cannot be suitably described from the viewpoint of strict weak coupling approaches, and adopting a picture of intermediate coupling is necessary. Rephrased in terms of diagrammatic expansions starting from the noninteracting problem, this amounts to investigating the leading *and* subleading divergent classes of diagrams. In particular, this is relevant for the competition between magnetic and SC phases in this kind of systems, one recent example of which has been the iron pnictides.[15,16]

Main results. In this Rapid Communication, we use the functional renormalization group (FRG) method[17–20] to study the competition between many-body states in graphene doped to the vicinity of the VHS. We analyze this problem at a level which provides a detailed connection to the experimental setup including both the possibility of long-range hopping and Coulomb interactions. From our analysis, we obtain a rich phase diagram which, depending on the range of chosen kinetic and interaction parameters, contains magnetic and different SC phases, summarized in Fig. 1. For a certain range of parameters described below, we find a $d + id$ SC phase which has been previously studied by the random phase approximation (RPA)[5,21] and 3RG.[14] To analyze all possible many-body phases and their dependence on the system parameters, FRG provides a systematic unbiased summation of diagrams in both particle-particle channels *and* particle-hole channels as well as vertex corrections, and keeps track of the whole Fermi surface [Fig. 2(a)]. We investigate in detail how different band structure parameters affect the phase diagram. We find that rather small variations of the longer-ranged hopping parameters such as next-nearest (t_2) and next-next-nearest (t_3) hopping can shift the position of perfect Fermi surface nesting against the VHS (Fig. 2). As we will see below, this significantly influences the competition between magnetism and SC. Moreover, away from the exact VHS, the reduced screening of the Coulomb interaction does not justify the assumption of a local Hubbard model description. For this

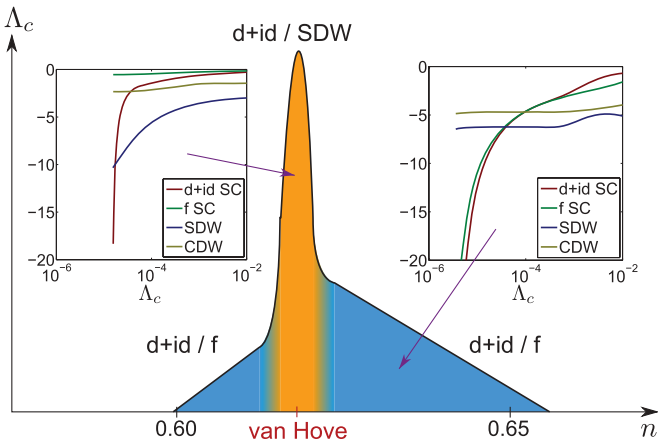

FIG. 1. (Color online) Phase diagram for graphene around van Hove filling as obtained by FRG. Λ_c serves as an upper bound for T_c as a function of doping. Left inset: Dominant $d+id$ instability at van Hove filling for $U_0 = 10$ eV and the band structure in Ref. 5. Away from van Hove filling [dark shaded (blue) area], Λ_c drops. Whether $d+id$- or f-wave SC instability is preferred depends on the long rangedness of the interaction (right inset: $U_1/U_0 = 0.45$ and $U_2/U_0 = 0.15$).

case, we find that longer-ranged Coulomb interactions[22] can significantly change the phase diagram, as CDW fluctuations become more competitive to SDW fluctuations, and a triplet SC phase can appear. In particular, we study how Cooper pairing in the different SC phases responds to differently long-ranged Coulomb interactions. Our results suggest that in experiment, modifications of the band structure such as imposed by pressure as well as by changing the dielectric environment of the graphene sample would enable the realization of different many-body states and possible phase transitions between them.

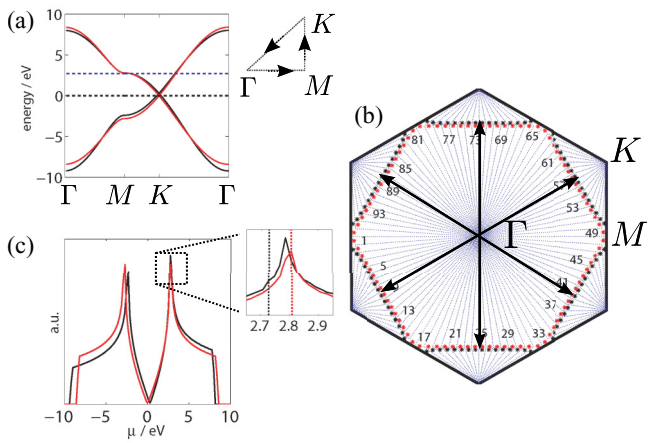

FIG. 2. (Color online) (a) Band structure of graphene for $t_1 = 2.8$ eV (red) and for $t_1 = 2.8$, $t_2 = 0.7$, $t_3 = 0.02$ eV (black). (b) Fermi surface near the van Hove point [dashed blue level in (a)], 96 patches ($\boldsymbol{k}$ points) used in the FRG and the nesting vector, and the partial nesting vectors. (c) DOS for both band structures in (a). Inset: Position shift of Fermi surface nesting (dashed vertical lines) vs the VHS peak.

Model. We consider the π band structure part of graphene approximated by a tight-binding model including up to third nearest neighbors on the hexagonal lattice:

$$H_0 = \Bigg[t_1 \sum_{\langle i,j\rangle} \sum_{\sigma} c^\dagger_{i,\sigma} c_{j,\sigma} + t_2 \sum_{\langle\langle i,j\rangle\rangle} \sum_{\sigma} c^\dagger_{i,\sigma} c_{j,\sigma} + t_3 \sum_{\langle\langle\langle i,j\rangle\rangle\rangle} \sum_{\sigma} c^\dagger_{i,\sigma} c_{j,\sigma} + \text{H.c.} \Bigg] - \mu n, \tag{1}$$

where $n = \sum_{i,\sigma} n_{i,\sigma} = \sum_{i,\sigma} c^\dagger_{i,\sigma} c_{i,\sigma}$, and $c^\dagger_{i,\sigma}$ denotes the electron creation operator of spin $\sigma = \uparrow, \downarrow$ at site i. The resulting band structure is a two-band model due to two atoms per unit cell (Fig. 2). There are uncertainties about the most appropriate tight-binding fit for graphene, in particular as it concerns the longer-ranged hybridization integrals.[1,23] For dominant t_1, the band structure features a van Hove singularity (VHS) at $n = 3/8, 5/8$. Constraining ourselves to the electron-doped case, the $n = 5/8$ electron-type Fermi surface is shown in Fig. 2(b). As depicted, this is the regime of enhanced DOS which is the focus in what follows. For $t_2 = t_3 = 0$ (red curve in Fig. 2), the VHS coincides with the partial nesting of different sections of the Fermi surface for $\boldsymbol{Q} = (0, 2\pi/\sqrt{3}), (\pi, \pi/\sqrt{3})$, and $(\pi, -\pi/\sqrt{3})$. For a realistic band structure estimate with finite t_2 and t_3 (Ref. 5) (black curve in Fig. 2), this gives a relevant shift of the perfect nesting position versus the VHS as well as DOS at the VHS, and affects the many-body phase found there.

We consider the long-range Hubbard Hamiltonian[22]

$$H_{\text{int}} = U_0 \sum_i n_{i,\uparrow} n_{i,\downarrow} + \frac{1}{2} U_1 \sum_{\langle i,j\rangle,\sigma,\sigma'} n_{i,\sigma} n_{j,\sigma'} + \frac{1}{2} U_2 \sum_{\langle\langle i,j\rangle\rangle,\sigma,\sigma'} n_{i,\sigma} n_{j,\sigma'}, \tag{2}$$

where $U_{0\ldots2}$ parametrizes the Coulomb repulsion scale from on-site to the second-nearest-neighbor interaction. It depends on the DOS how strongly the Coulomb interaction is screened. At the VHS, we assume perfect screening and consider the local limit U_0 only, while away from the VHS, we investigate the effects of taking U_1 and U_2 into consideration. The typical scale of the effective local repulsion has been found to be $U_0 \sim 10$ eV $< W$,[22] where $W \sim 17$ eV is the kinetic bandwidth.

Method. We employ the FRG and study how the renormalized interaction described by the 4-point function (4PF) evolves under integrating out high-energy fermionic modes: $V_\Lambda(\boldsymbol{k}_1; \boldsymbol{k}_2; \boldsymbol{k}_3; \boldsymbol{k}_4) c^\dagger_{\boldsymbol{k}_4 s} c^\dagger_{\boldsymbol{k}_3 \bar{s}} c_{\boldsymbol{k}_2 s} c_{\boldsymbol{k}_1 \bar{s}}$, where the temperature-flow parameter is the IR cutoff Λ approaching the Fermi surface, and $\boldsymbol{k}_1$ to $\boldsymbol{k}_4$ the incoming and outgoing momenta. Within the numerical treatment, the $\boldsymbol{k}$'s are discretized to take on the values representing the different patches of the Brillouin zone. Figure 2(b) shows a 96 patching scheme. The starting conditions of the RG are given by the bandwidth W serving as an UV cutoff, with the bare initial interactions for the 4PF. Due to the spin rotational invariance of interactions (we neglect spin-orbit coupling in our analysis), we constrain ourselves to the $S^z = 0$ subspace of incoming momenta $\boldsymbol{k}_1, \boldsymbol{k}_2$ (and outgoing $\boldsymbol{k}_3, \boldsymbol{k}_4$) and generate the singlet and triplet

channel by symmetrization and antisymmetrization of the 4PF V_Λ.[19] The diverging channels of the 4PF under the flow to the Fermi surface signal the nature of the instability, and the corresponding Λ_c, as a function of some given system parameter such as doping, gives the same qualitative behavior as T_c. At a cutoff scale where the leading instability starts to diverge, we then decompose the different channels such as SC or SDW into eigenmode contributions and obtain the form factors associated with the instabilities.[15,24]

Phase diagram. The phase diagram as a function of doping, obtained for realistic microscopic kinetic and interaction parameters,[5,22] is shown in Fig. 1. At the same time, however, we also investigate trends how the system evolves when we tune the parameters away from this setting. At the VHS (orange-shaded area in Fig. 1), the DOS is so large that a local Hubbard description is appropriate. (The conclusions drawn here also persist as small long-range Coulomb components would be taken into account at exact van Hove filling.) For realistic $U_0 \sim 10$ eV, we find that the $d+id$ SC instability is dominant, assuming finite hopping parameters $t_2 = 0.1$ eV and $t_3 = 0.07$ eV.[1] (The result is rather similar for the values of Ref. 23.) Only at scales of $U_0 > 18$ eV, the SDW becomes dominant for this scenario. Note, however, that only small modifications of the band structure can strongly affect the competition of SDW and SC at the VHS: When t_2 is reduced, the system gets more biased to the SDW, as the SDW fluctuations in the nesting channel get enhanced. For t_1 only [red curve in Fig. 2(a)], the SDW already wins for $U_0 > 8.5$ eV, and can give rise to a helical magnet scenario. As we move away from the VHS (blue-shaded area in Fig. 1), details of the band structure become less relevant, and we note that the critical instability scale Λ_c drops more strongly towards the Dirac point than away from it, mainly as a consequence of the reduced DOS. As SDW fluctuations are weakened, SC phases become dominant. Assuming rather local Coulomb interactions ($U_1/U_0 < 0.5$), we find that the system still favors the $d+id$ SC state. Allowing for more long-ranged Hubbard interactions, however, the picture changes: The CDW fluctuations are comparable to the SDW fluctuations which bias the system towards singlet SC, and triplet f-wave pairing becomes competitive.

$d+id$-wave phase. We analyze the d-wave SC phase at the VHS (U_0 only) in more detail. The honeycomb lattice is characterized by C_{6v} symmetry about the center of hexagons, and the SC order parameter transforms as one of the irreducible representations. $d_{x^2-y^2}$ and d_{xy} waves follow the two-dimensional E_2 representation and are hence degenerate. The different form factors are plotted in Fig. 3(a). We find that the numerical solutions can be fit to $f[d_{x^2-y^2}] = 2\cos(\sqrt{3}k_y) - \cos[(\sqrt{3}k_y - 3k_x)/2] - \cos[(\sqrt{3}k_y + 3k_x)/2]$ and $f[d_{xy}] = \cos[(\sqrt{3}k_y - 3k_x)/2] - \cos[(\sqrt{3}k_y + 3k_x)/2]$. From the Fourier transform of the momentum-resolved form factors $f(\boldsymbol{k})$ along the Fermi surface, we also obtain the pairing amplitudes of the real space SC pairing function[25] (Fig. 3). The Cooper pairing emerges on nearest neighbors of the same hexagonal sublattice. As we move to the broader vicinity of the VHS, where we assume a longer-ranged Hubbard interaction, the form factors retain the d-wave E_2 representation, while the Cooper-pair wave function

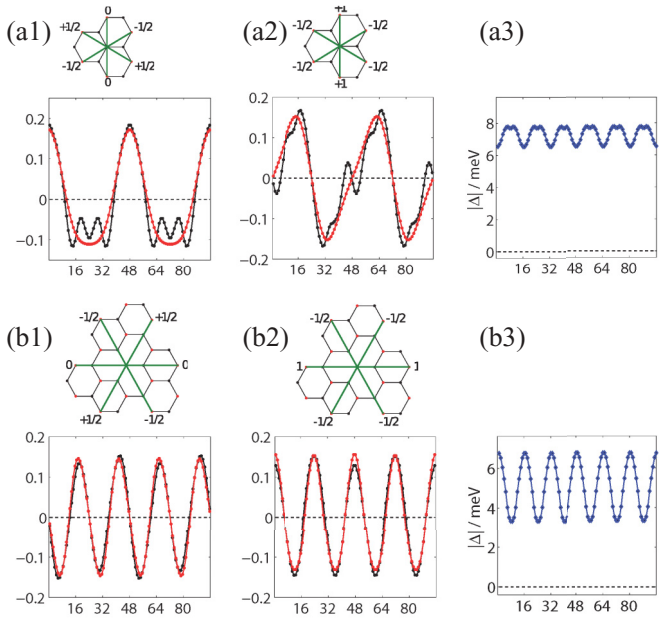

FIG. 3. (Color online) $d_{x^2-y^2}$- and d_{xy}-wave solutions for (a) $U_0 = 10$ eV only and (b) $U_1/U_0 = 0.45$, $U_2/U_0 = 0.15$. (a1),(a2) and (b1),(b2) show the form factors of $d_{x^2-y^2}$ and d_{xy} plotted along the Fermi surface according to patch indices defined in Fig. 2(b), as well as the real space pair amplitude patterns. The solutions change from (a) to (b). The analytic form factors given in the text (red) fit the numerical data (black). (a3) and (b3) show the gap profile of $d+id$ along the Fermi surface (the actual connection to experimental energy scale can still vary by a global factor). The gap anisotropy increases from (a) to (b).

changes as shown in Fig. 3(b) ($U_1/U_0 = 0.4$, $U_2/U_0 = 0.15$). There, the form factors change to $f[d_{x^2-y^2}] = 2\cos(3k_x) - \cos[(3\sqrt{3}k_y - 3k_x)/2] - \cos[(3\sqrt{3}k_y + 3k_x)/2]$ and $f[d_{xy}] = \cos[(3\sqrt{3}k_y - 3k_x)/2] - \cos[(3\sqrt{3}k_y + 3k_x)/2]$, corresponding to a doubled number of nodes along the Fermi surface. From the pairing amplitudes, we also observe that the pairing spreads out to the second nearest neighbor of the same sublattice. This is a consequence of the long-range Coulomb interactions: The Cooper-pair wave function seeks to develop more nodes to minimize Coulomb repulsion, and is able to do so by longer-ranged Cooper pairing. This, however, still does not tell us about the gap function of the d-wave instability. As the degeneracy is protected by symmetry, the system could generically form any linear combination $d_{x^2-y^2} + e^{i\theta} d_{xy}$ of both d-wave solutions. We hence perform a mean-field decoupling in the SC pairing channel and minimize the free energy. The necessary condition for the minimum is rephrased by the self-consistent gap equation[26]

$$\Delta_{\boldsymbol{q}} = -1/N \sum_{\boldsymbol{k}} V_\Lambda^{\mathrm{SC}}(\boldsymbol{k},\boldsymbol{q}) \frac{\Delta_{\boldsymbol{k}}}{2E(\boldsymbol{k})} \tanh\left(\frac{E(\boldsymbol{k})}{2T}\right), \qquad (3)$$

where $V_\Lambda^{\mathrm{SC}}(\boldsymbol{k},\boldsymbol{q})$ is the 4PF in the pairing channel taken at a cutoff $\Lambda_c \sim T_c$. The gap functions are displayed in Figs. 3(a3) and 3(b3). We always find $d+id$ to be the energetically preferred state. This is rather generic in a situation of degenerate nodal SC order parameters, since such a combination allows the system to avoid nodes in the gap function. The gaps we find

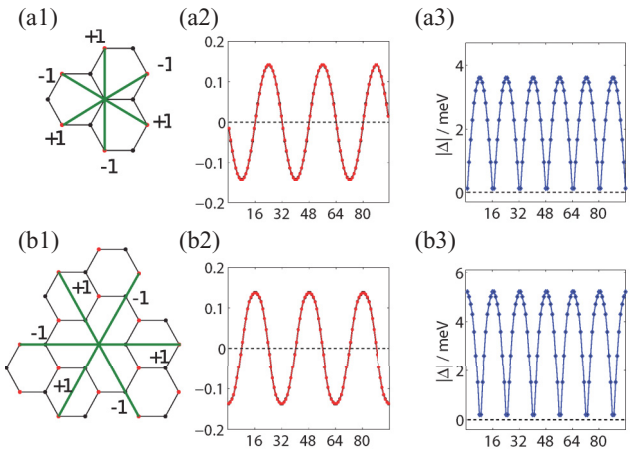

FIG. 4. (Color online) Pairing amplitudes, form factors, and gap profiles for the f-wave phase as defined in Fig. 3, representative for larger fillings than the VHS for (a) $U_1/U_0 = 0.6$ to (b) $U_1/U_0 = 0.6$, $U_2/U_0 = 0.2$. The gap profile is nodal, and the nodal points shift from (a) to (b).

are hence nodeless and only slightly change their anisotropy as the pairing function varies [Figs. 3(a) and 3(b)]. As graphene can be tuned rather accurately to the van Hove filling (where we find the highest critical scale), it may be a reasonably accessible experimental system to study such a SC phase. The expected experimental evidence for $d + id$ would be a nodeless gap detectable through transport measurements and singlet pairing due to a Knight shift drop below T_c. A minor caveat is given by the role of impurities which may spoil the symmetry between the two d-wave solutions. This could give rise to a nodal gap beyond sufficient impurity concentration.[27]

f-wave phase. It is similarly interesting to investigate the triplet f-wave instability[28] which dominates for longer-ranged Coulomb interaction (Fig. 4). It obeys the one-dimensional B_1 or B_2 representation, depending on the range of the Coulomb interaction. For $U_1/U_0 = 0.6$, the form factor and pairing amplitudes are plotted in Fig. 4(a) as well as for $U_1/U_0 = 0.6$, $U_2/U_0 = 0.2$ in Fig. 4(b). We again find that the Cooper-pair distance increases with longer-ranged interactions, which manifests itself as a change of the form factor $f[f_{B_1}] = \sin(\sqrt{3}k_y) - 2\sin(\sqrt{3}k_y/2)\cos(3k_x/2)$ in Fig. 4(a) to $f[f_{B_2}] = \sin(3k_x) - 2\sin(3k_x/2)\cos(3\sqrt{3}k_y/2)$ in Fig. 4(b). The gap function follows the absolute value of the form factor, showing a nodal gap, where the points of the nodes change with increasing Coulomb range. In the case of the f-wave, the position of the nodes would hence indicate the Cooper-pairing distance associated with the long-range properties of the Coulomb interaction, and suggest experimental evidence of a nodal gap from transport and an invariant Knight shift due to triplet pairing. For fillings smaller than the VHS, the Fermi surface is disconnected and the nodes might not coincide with the Fermi surfaces. This f-wave regime is very low in T_c, depending on preference for B_1 or B_2, and may be nodeless.

Summary and outlook. In summary, we have provided a detailed analysis of the competing many-body phases of graphene at and around van Hove filling. We find that, for realistic band-structure parameters and interactions, the exotic nodeless singlet $d + id$-wave SC phase is preferred over an extended phase space regime around the VHS. Variations of the kinetic parameters and effective interaction scales can drive a transition to a spin-density-wave (helical magnet) phase at the van Hove point. Away from the VHS, reduced Coulomb screening and, thus, longer-ranged Coulomb interactions change the form of the $d + id$ Cooper-pair wave function, and in certain limits can favor a nodal triplet f-wave SC phase.

The possibility of the time-reversal symmetry breaking $d + id$ phase in graphene is very intriguing: It has been noted early on in the context of the cuprates that such a phase would have various interesting properties such as quantized edge currents.[29,30] Furthermore, provided a Rashba spin-orbit interaction is present, the $d + id$ phase supports Majorana modes in the vortex cores obeying non-Abelian statistics.[31] The tunability of the Rashba interaction in graphene[32] may enable realization of the Majorana modes; due to the two-dimensional nature of graphene and its tunability, their observation and manipulation should be easier than in other materials.

We gratefully acknowledge discussions with A. Chubukov, C. Honerkamp, G. Baskaran, S. Raghu, L. Boeri, and S.-C. Zhang. M.L.K. is supported by DFG-FOR 1162. C.P., W.H., and R.T. are supported by DFG-SPP 1458/1, and C.P. by DFG-FOR 538. R.T. is supported by an SITP fellowship of Stanford University.

[1] A. H. Castro Neto, F. Guinea, N. M. R. Peres, K. S. Novoselov, and A. K. Geim, Rev. Mod. Phys. **81**, 109 (2009).
[2] V. N. Kotov, B. Uchoa, V. M. Pereira, A. H. C. Neto, and F. Guinea, Rev. Mod. Phys. **84**, 1067 (2012).
[3] J. Gonzalez, F. Guinea, and M. A. H. Vozmediano, Phys. Rev. B **59**, R2474 (1999).
[4] J. Gonzalez, F. Guinea, and M. A. H. Vozmediano, Nucl. Phys. B **424**, 595 (1994).
[5] J. L. McChesney, A. Bostwick, T. Ohta, T. Seyller, K. Horn, J. González, and E. Rotenberg, Phys. Rev. Lett. **104**, 136803 (2010).
[6] D. K. Efetov and P. Kim, Phys. Rev. Lett. **105**, 256805 (2010).
[7] B. Uchoa and A. H. Castro Neto, Phys. Rev. Lett. **98**, 146801 (2007).
[8] B. Roy and I. F. Herbut, Phys. Rev. B **82**, 035429 (2010).
[9] C. Honerkamp, Phys. Rev. Lett. **100**, 146404 (2008).
[10] G. Baskaran, Phys. Rev. B **65**, 212505 (2002).
[11] A. M. Black-Schaffer and S. Doniach, Phys. Rev. B **75**, 134512 (2007).
[12] S. Pathak, V. B. Shenoy, and G. Baskaran, Phys. Rev. B **81**, 085431 (2010).
[13] M. Calandra and F. Mauri, Phys. Rev. Lett. **95**, 237002 (2005).

[14]R. Nandkishore, L. Levitov, and A. Chubukov, Nat. Phys. **8**, 158 (2012).
[15]R. Thomale, C. Platt, W. Hanke, and B. A. Bernevig, Phys. Rev. Lett. **106**, 187003 (2011).
[16]S. Maiti and A. V. Chubukov, Phys. Rev. B **82**, 214515 (2010).
[17]D. Zanchi and H. J. Schulz, Phys. Rev. B **61**, 13609 (2000).
[18]C. J. Halboth and W. Metzner, Phys. Rev. B **61**, 7364 (2000).
[19]C. Honerkamp, M. Salmhofer, N. Furukawa, and T. M. Rice, Phys. Rev. B **63**, 035109 (2001).
[20]W. Metzner, M. Salmhofer, C. Honerkamp, V. Meden, and K. Schönhammer, Rev. Mod. Phys. **84**, 299 (2012).
[21]J. Gonzalez, Phys. Rev. B **78**, 205431 (2008).
[22]T. O. Wehling, E. Sasioglu, C. Friedrich, A. I. Lichtenstein, M. I. Katsnelson, and S. Blugel, Phys. Rev. Lett. **106**, 236805 (2011).
[23]S. Reich, J. Maultzsch, C. Thomsen, and P. Ordejón, Phys. Rev. B **66**, 035412 (2002).
[24]H. Zhai, F. Wang, and D.-H. Lee, Phys. Rev. B **80**, 064517 (2009).
[25]P. Sahebsara and D. Senechal, arXiv:0908.0474.
[26]C. Platt, R. Thomale, C. Honerkamp, S.-C. Zhang, and W. Hanke, Phys. Rev. B **85**, 180502 (2012).
[27]S. Florens and M. Vojta, Phys. Rev. B **71**, 094516 (2005).
[28]S. Raghu, S. A. Kivelson, and D. J. Scalapino, Phys. Rev. B **81**, 224505 (2010).
[29]R. B. Laughlin, Phys. Rev. Lett. **80**, 5188 (1998).
[30]M. Sigrist and K. Ueda, Rev. Mod. Phys. **63**, 239 (1991).
[31]M. Sato, Y. Takahashi, and S. Fujimoto, Phys. Rev. B **82**, 134521 (2010).
[32]H. Min, J. E. Hill, N. A. Sinitsyn, B. R. Sahu, L. Kleinman, and A. H. MacDonald, Phys. Rev. B **74**, 165310 (2006).